

DeepCell: Multiview Representation Learning for Post-Mapping Netlists

Zhengyuan Shi^{1,5§}, Chengyu Ma^{2,5§}, Ziyang Zheng^{1,5}, Lingfeng Zhou^{3,5}, Hongyang Pan^{4,5}, Wentao Jiang^{2,5},
Fan Yang⁴, Xiaoyan Yang³, Zhufei Chu² and Qiang Xu^{1,5}

¹*Department of Computer Science and Engineering, The Chinese University of Hong Kong, Sha Tin, Hong Kong S.A.R.*

²*Faculty of Electrical Engineering and Computer Science, Ningbo University, Ningbo, China*

³*School of Computer Science, Hangzhou Dianzi University, Hangzhou, China*

⁴*School of Microelectronics, State Key Laboratory of Integrated Chips and System, Fudan University, Shanghai, China*

⁵*National Center of Technology Innovation for EDA, Nanjing, China*

Abstract—Representation learning for post-mapping (PM) netlists is a critical challenge in Electronic Design Automation (EDA), driven by the diverse and complex nature of modern circuit designs. Existing approaches focus on intermediate representations like And-Inverter Graphs (AIGs), limiting their applicability to post-synthesis stages. We introduce *DeepCell*, a multiview representation learning framework that integrates structural and functional insights from both PM netlists and AIGs to learn rich, generalizable embeddings. At its core, DeepCell employs the novel Mask Circuit Modeling (MCM) mechanism, which refines PM netlist representations in a self-supervised manner using pretrained AIG encoders. DeepCell sets a new benchmark in PM netlist representation, outperforming existing methods in predictive accuracy and reconstruction fidelity. To validate its efficacy, we apply DeepCell to functional Engineering Change Orders (ECO), achieving significant reductions in patch generation costs and runtime while improving patch quality.

Index Terms—circuit representation learning, mask modeling, multiview learning, engineering change order (ECO)

I. INTRODUCTION

Representation learning has emerged as a powerful paradigm across domains such as computer vision (CV) and natural language processing (NLP), where pretrained models finetuned for specific tasks achieve state-of-the-art results. Inspired by these advancements, the field of Electronic Design Automation (EDA) has explored similar methodologies for circuit representation learning. Existing approaches, such as DeepGate Family [1], [2], FGNN [3], Gamora [4] and HOGA [5], demonstrate significant improvements in tasks like testability analysis, circuit identification, and design verification by focusing on And-Inverter Graphs (AIGs). However, this narrow reliance on AIGs limits their generalization to more complex and practical circuit abstractions.

Post-mapping (PM) netlists, composed of diverse standard cells, represent a key stage in the design flow but remain underexplored in circuit representation learning. These netlists introduce challenges due to their structural and functional heterogeneity, which is difficult to be effectively captured by existing AIG-based methods. Current solutions, such as simulation-based supervised training [2] or contrastive learning [3], struggle with scalability and efficiency in handling PM

netlists. This gap hinders progress in critical post-mapping tasks like technology mapping and functional Engineering Change Orders (ECO).

To address these challenges, we propose **DeepCell**, a novel multiview representation learning framework for PM netlists. DeepCell integrates information from both PM netlists and AIGs using a Graph Neural Network (GNN)-based PM encoder and a pretrained AIG encoder. At its core, DeepCell employs *Mask Circuit Modeling (MCM)*, a self-supervised mechanism inspired by Masked Language Modeling (MLM) [6], which leverages AIG embeddings to refine PM netlist representations. By bridging the structural-functional gap inherent in PM netlists, DeepCell achieves rich and generalizable embeddings. We then validate DeepCell through its application to the functional ECO task, a critical post-mapping challenge involving design modification after tape-out [7]. Integrated as a plug-in to an existing ECO tool, DeepCell significantly reduces patch generation costs and runtime.

Our contributions are summarized as follows:

- We propose DeepCell, the first multiview and multi-modal representation learning framework tailored for PM netlists, integrating structural and functional insights from diverse standard cells.
- We introduce Mask Circuit Modeling (MCM), a self-supervised mechanism for refining PM netlist embeddings using AIG-based representations.
- We demonstrate the utility of DeepCell in functional ECO, achieving reductions in patch generation costs, gate count, and runtime while maintaining high-quality results.

The remainder of this paper is organized as follows: Section II reviews related work. Section III describes the proposed DeepCell framework, including architecture and Mask Circuit Modeling mechanism. Section IV presents the pretraining results and investigate the effect of proposed training strategy. Next, we apply DeepCell in functional ECO tasks. Finally Section VI concludes this paper.

II. RELATED WORK

A. Circuit Representation Learning

Circuit representation learning has emerged as an attractive direction in the field of EDA, focusing on training models

[§]Both authors contributed equally to this research.

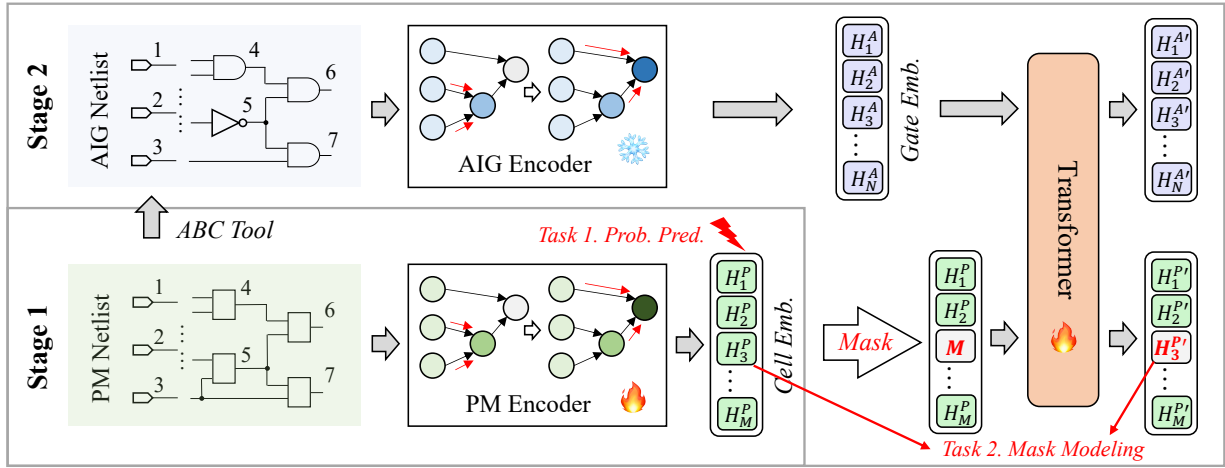


Fig. 1. Overview of DeepCell

to obtain general circuit embeddings that can be applied to various downstream tasks [8]. The first circuit representation learning framework, DeepGate [1], proposes supervising model training using logic-1 probability under random simulation and achieves substantial improvements in tasks like testability analysis [9] and power estimation [10]. Its successor, DeepGate2 [2], further refines this approach by separating functional and structural embeddings for different applications. Additionally, Gamora [4] and HOGA [5] leverage sub-circuit identification as pre-training tasks, while FGNN [3] trains models in an unsupervised contrastive manner by distinguishing between equivalent and non-equivalent circuits. Despite these advancements, existing models primarily focus on learning representations of AIG netlists. There is still no available solution capable of learning post-mapping netlists with arbitrary logic cells and addressing the practical applications on post-mapping stages.

While these advancements primarily address representation learning for intermediate formats such as AIGs, the challenges posed by post-mapping netlists remain largely unexplored. Functional ECO represents one such critical post-mapping application, where effective representation learning could significantly enhance performance and efficiency.

B. Functional ECO

ECO are a critical component in the VLSI design process, used to rectify design problems after tape-out or chip fabrication. ECO involve making modifications to correct these errors, and they are indispensable in avoiding the high expenses associated with design re-spin [11]. For functional ECO, the purpose is to generate patch so that the original circuit is equal to the golden circuit, while minimizing the resource cost of the generated patches and making the running time as short as possible. Synthesis-based ECO algorithms are good at solving this problem [7]. It relies on a diagnostic strategy to identify internal rectifier signals, and then applies a resynthesis technique to generate patch functions for functional differences. These algorithms have been able to automate the process of functional ECO.

III. METHODOLOGY

A. Overview

Fig. 1 presents the overview of DeepCell framework, which consists of an AIG encoder, a PM encoder and a Transformer model. The framework operates in two stages to capture the general representation of post-mapping (PM) netlists. In Stage 1, the PM encoder is trained to learn cell embeddings (*Cell Emb.*) from the PM netlist. In Stage 2, the AIG encoder, which has been pretrained and frozen, is utilized to extract gate embeddings (*Gate Emb.*) from the corresponding AIG netlist. Then, we mask a random subset of the cell embeddings and reconstruct these masked embeddings using the gate embeddings.

B. PM Encoder

Given a PM netlist, we convert it into graph format $\mathcal{G}^P = (\mathcal{V}^P, \mathcal{E}^P)$, where each standard cell is represented as node and each wire is treated as edge on the graph.

1) *Node Features*: PM netlists consist of a wide variety of standard cells, making it impractical to represent them using one-hot encoding for each type of cell. Therefore, To address this, we embed the truth table of each standard cell into its corresponding node feature x_i . Formally, the node feature encoding is defined in in Eq. (1), where D is the dimension of node feature vector and tt_i represents the 0/1 truth table vector of standard cell i . The truth table tt_i is repeated until the node feature vector reaches the specified dimension D . In the default setting, we assign $D = 64$, ensuring that this encoding mechanism is adaptable to PM netlists across various technology libraries and supports arbitrary logic units with up to 6 inputs.

$$x_i = \text{repeat}(tt_i, D) \quad (1)$$

For example, the cell `xor2_1` defines XOR functionality with 2 inputs and 1 output. Its truth table, 0110, is extracted from the technology library and expanded into a 64-dimensional feature vector by repeating the pattern. Thus, the node feature of the `xor2_1` cell becomes 0110 0110 ... 0110.

2) *Aggregator*: We introduce a DAG-based GNN to encode circuit graph into embedding vectors \mathbf{H}^P . For each cell $i \in \mathcal{V}^P$, its representation vector is denoted as $H_i^P = \{hs_i^P, hf_i^P\}$, where hs_i^P and hf_i^P are the structural and functional embeddings, $H_i^P \in \mathbf{H}^P$. To compute these embeddings, we propose two aggregators: $aggr^s$ for structural message aggregation and $aggr^f$ for functional message aggregation.

For structural embedding aggregation, $aggr^s$ is implemented using the GCN aggregator [12], which aggregates messages from the predecessors of i . Here, $\mathcal{P}(i)$ denotes the set of fanin cells of i :

$$hs_i = aggr^s(\{hs_j | j \in \mathcal{P}(i)\}) \quad (2)$$

For functional embedding aggregation, $aggr^f$ is implemented using a self-attention aggregator [13] to distinguish the functionality of the predecessors. Unlike AIG netlists, which consist solely of AND gates and inverters, PM netlists contain diverse standard cells. To account for this diversity, we differentiate cells using their node features x_i and introduce an update function, *update*. Formally, the functional aggregation process in DeepCell is defined as Eq. (3), with the *update* function implemented as a multi-layer perceptron (MLP).

$$\begin{aligned} msg_i &= aggr^f(\{cat(hs_j, hf_j) | j \in \mathcal{P}(i)\}) \\ hf_i &= update(msg_i, x_i) \end{aligned} \quad (3)$$

Finally, the embeddings of PM netlist are denoted as Eq. (4), where *encoder* is the above GNN-based PM encoder.

$$\begin{aligned} \mathbf{H}^P &= encoder(\mathcal{G}^P) \\ H_i^P &\in \mathbf{H}^P, i \in \mathcal{V}^P \end{aligned} \quad (4)$$

C. AIG Encoder

Our DeepCell framework incorporates a multiview representation learning mechanism, enabling it to learn cell embeddings in PM netlists from an additional perspective provided by AIGs. Specifically, given a PM netlist $\mathcal{G}^P = (\mathcal{V}^P, \mathcal{E}^P)$, we convert it into an AIG netlist $\mathcal{G}^A = (\mathcal{V}^A, \mathcal{E}^A)$. We then employ DeepGate2 [2] as the AIG encoder to derive the gate-level embeddings $H_j^A \in \mathbf{H}^A$ as formulated in Eq. (5).

$$\begin{aligned} \mathbf{H}^A &= DeepGate2(\mathcal{G}^A) \\ H_j^A &\in \mathbf{H}^A, j \in \mathcal{V}^A \end{aligned} \quad (5)$$

D. Mask Circuit Modeling

We refine the cell embeddings \mathbf{H}^P using information from the AIG view by mask circuit modeling (MCM). As shown in Fig. 2, given a PM netlist \mathcal{G}^P , we convert \mathcal{G}^P to AIG Netlist \mathcal{G}^A . Both \mathcal{G}^P and \mathcal{G}^A are encoded by PM encoder and AIG encoder in Eq. (4) and Eq. (5), respectively.

To apply MCM, we randomly select node $p \in \mathcal{G}^P$ and extract a k -hop predecessors around node p , denoted as the masked hop $\mathcal{M}(p)$. Within the masked hop $\mathcal{M}(p)$, we replace the functional embeddings hf_i of the nodes with a learnable masked token hm , while preserving their structural embeddings hs_i .

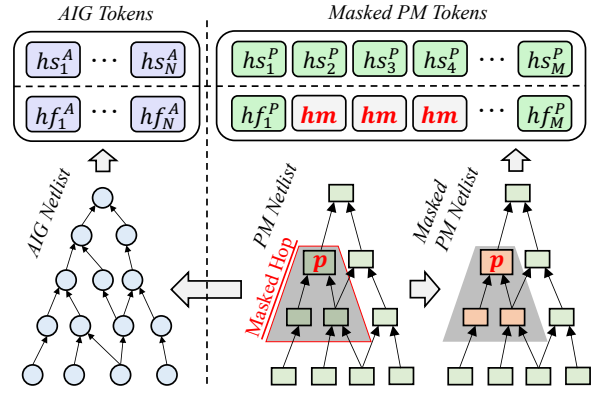


Fig. 2. Mask Circuit Modeling

Therefore, we totally have $M + N$ tokens (see Eq. (6)), where $M = |\mathcal{V}^P|$ and $N = |\mathcal{V}^A|$. All the selected masked nodes p is in set \mathcal{S} .

$$\begin{aligned} H_i^P &= \{hs_i^P, hf_i^P\}, i \in \mathcal{V}^P, i \notin \mathcal{M}(p) \\ H_i^P &= \{hs_i^P, hm\}, i \in \mathcal{V}^P, i \in \mathcal{M}(p) \\ H_j^A &= \{hs_j^A, hf_j^A\}, j \in \mathcal{V}^A \end{aligned} \quad (6)$$

We process these $M + N$ tokens using a Transformer model \mathcal{T} . Formally, we define the input and output of the Transformer model as below. The training objective is to reconstruct the masked area using the remaining cell embeddings and the learned gate embeddings from AIG view.

$$\{\mathbf{H}^{A'}, \mathbf{H}^{P'}\} = \mathcal{T}(\{\mathbf{H}^A, \mathbf{H}^P\}) \quad (7)$$

E. Model pretaining

To train DeepCell, we employ a two-stage training strategy. As illustrated in Fig. 1, in the first stage, we perform random simulation with 15,000 patterns on PM netlist and record the logic-1 probability $prob_i, i \in \mathcal{V}^P$. Next, we use a simple 3-layer MLP to readout the functional embeddings as the predicted probability. The training loss for this stage is defined in Eq. (8).

$$\begin{aligned} \hat{prob}_i &= MLP(hf_i), i \in \mathcal{V}^P \\ loss_{prob} &= L1Loss(prob_i, \hat{prob}_i) \end{aligned} \quad (8)$$

In the second stage, we refine the cell embeddings by incorporating representations from the AIG view. We utilize a pretrained and frozen AIG encoder to provide rich contextual information from the AIG. The training objective in this stage is to reconstruct the functionality of masked cells using information from their neighboring cells and the global AIG perspective. Accordingly, we define the MCM training loss in Eq. (9), where the model is trained to recover the functional embeddings of the masked cells.

$$loss_{mcm} = L1Loss(H_i^P, H_i^{P'}) \quad (9)$$

Consequently, the overall loss functions for both stages are defined as follows, where w_{prob} and w_{mcm} present the weights

of these two training tasks. We assign $w_{prob} = 1$ and $w_{mcm} = 1$ in default setting.

$$\begin{aligned} L_{stage1} &= loss_{prob} \\ L_{stage2} &= w_{prob} \cdot loss_{prob} + w_{mcm} \cdot loss_{mcm} \end{aligned} \quad (10)$$

IV. EXPERIMENTS

In this section, we train our DeepCell to learn the general representations of standard cells in the post-mapping netlists.

A. Experiment Settings

1) *Data Preparation*: We collect the open-source verilog designs from GitHub and the open-source circuit benchmarks [14]–[16]. All circuits are designed with Skywater 130nm as the target process library [17], using commercial logic synthesis tool Design Compiler command `compile_ultra` to obtain the corresponding PM netlist. To accelerate model pretraining, we randomly extract the sub-circuits within 5,000 cells. Then, we use ABC `strash` command to obtain the corresponding AIGs. Consequently, there are totally 83,155 PM netlists and corresponding AIGs. We split the dataset into 80% for training and 20% for testing.

2) *Evaluation Metrics*: In the following experiments, we evaluate model performance in predicting the logic-1 probability under random simulation, a widely used metric for assessing circuit representation ability [1], [18]. We calculate the average prediction error (PE) as Eq. (11).

$$PE = \frac{1}{|\mathcal{V}^P|} \sum_{i \in \mathcal{V}^P} |prob_i - \hat{prob}_i| \quad (11)$$

Additionally, we assess model performance on mask circuit modeling tasks, where the average reconstruction error (RE) is defined as Eq. (12), where all the select nodes p are in set \mathcal{S} and the masked hop is $\mathcal{M}(p)$.

$$RE = \frac{1}{\sum |\mathcal{M}(p)|} \sum_{i \in \mathcal{M}(p)} |hf_i^P - hf_i^{P'}|, p \in \mathcal{S} \quad (12)$$

3) *Model Implementation and Training*: The Transformer model used to refine cell embeddings consists of 4 Transformer blocks, each with 8 attention heads. After encoding, each cell is represented by a 128-dimensional structural embedding and a 128-dimensional functional embedding. DeepCell is pretrained for 60 epochs in Stage 1 and an additional 60 epochs in Stage 2 to ensure convergence. The pretraining process is conducted with a batch size of 128 using 8 Nvidia A800 GPUs. We employ the Adam optimizer with a learning rate of 10^{-4} .

B. Experimental Results

1) *Effect of Mask Modeling*: We investigate the optimal settings for Mask Circuit Modeling (MCM) by exploring its two key hyperparameters: the number of selected nodes to be masked, $|\mathcal{S}|$, and the size of the masked hop, k . To evaluate performance, we pretrain the model using various hyperparameter combinations, where $|\mathcal{S}| = \theta \cdot |\mathcal{V}^P|$ and $\theta = 1\%, 5\%, 10\%, 20\%$ of total nodes in PM netlist, with hop sizes of $k = 4$ or $k = 6$.

TABLE I
EFFECT OF MASK MODELING

θ	$k = 4$		$k = 6$	
	PE	RE	PE	RE
0.01	0.0322	0.0099	0.0380	0.0211
0.05	0.0323	0.0097	0.0418	0.0257
0.10	0.0334	0.0110	0.0552	0.0794
0.20	0.0446	0.0398	0.0682	0.1035

TABLE II
EFFECT OF MULTIVIEW LEARNING

		PE	RE
GCN [12]	w/o multiview	0.0956	-
	w/ multiview	0.0529	0.0571
GAT [13]	w/o multiview	0.1466	-
	w/ multiview	0.0682	0.0869
DeepCell	w/o multiview	0.0564	-
	w/ multiview	0.0323	0.0097

Table I presents the results for different values of θ and k . First, the reconstruction error (RE) increases with a larger masking hop size. For example, when $\theta = 0.05$, the RE for $k = 6$ is 0.0257, which is 164.95% higher than that for $k = 4$ (RE=0.0097). Second, masking a smaller number of nodes consistently reduces both the RE and PE. However, using a smaller θ makes the task less challenging and diminishes its effectiveness as a pretraining objective. Based on these observation, we select $\theta = 0.05$ and $k = 4$ as a trade-off between task complexity and model performance in the following experiments.

2) *Effect of Multiview Learning*: We investigate the impact of incorporating the AIG view on training our PM netlist representation model. To evaluate the representation capability of the DeepCell framework, we use the PE as the primary metric. Specifically, we compare the full multiview MCM training strategy (w/ multiview) with a baseline that uses only the PM encoder without refining embeddings through multiview training (w/o multiview). The RE metric is not available in the w/o multiview setting. It is important to note that the DeepCell w/o multiview setting reflects the representation capability of DeepGate2 [2] on PM netlists, since our DeepCell utilizes a similar aggregator in the PM encoder.

To the best of our knowledge, no prior work has focused on learning a general representation of PM netlists composed of standard cells. In addition to evaluating DeepCell, we also employ general Graph Neural Network (GNN) models, such as GCN [12] and GAT [13], as PM encoders to investigate the impact of MCM training.

Table II compares the performance of the models with and without multiview training. First, compared to other PM encoders, whether using multiview training or not, DeepCell outperforms alternatives such as GCN [12] and GAT [13], achieving the lowest PE of 0.0323. Second, DeepCell effectively reconstructs functional embeddings by leveraging surrounding cell embeddings and additional gate embeddings from the AIG, achieving an average RE of 0.0097. Third, all

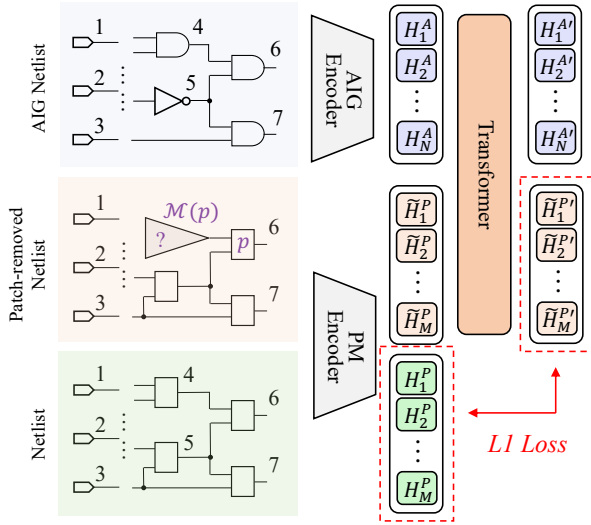


Fig. 3. Finetuning for ECO Application

models with multiview training outperform their counterparts without multiview training in terms of PE. For example, DeepCell with multiview training reduces PE by 42.7%, from 0.0564 to 0.0323. These results demonstrate the effectiveness of the proposed multiview representation learning mechanism for PM netlists.

V. DOWNSTREAM TASK: FUNCTIONAL ECO

In this section, we combine our DeepCell with the open-source EDA tools and apply our model to practical EDA tasks: functional ECO. Our DeepCell provides probability for nodes in the original circuit and provides guidance for ECO to find candidate patch signals. This method effectively leaves higher quality and more likely to be a patch signal, making the ECO solution more rapid and higher quality.

A. Preliminary

In order to clarify the role of the model in the algorithm, we first briefly describe the method in [19]. In the original SAT-based solution, for the POs reachable from the target, the method simultaneously identifies the PIs contained in these POs in the original netlist and the target netlist. Then find all signals in the original circuit, which are not in the transitive fanout cone of the targets and whose support is contained in the calculated set of PIs. These candidate signals are sorted by cost in ascending order and a fixed number of nodes (default is the top 5,000) are selected. Then used the SAT-based solution for the single-target ECO problem proposed in [20] to prove whether there is a solution.

After adding a large number of candidate signals, it is very expensive to use the positive and negative remainders of target to construct the miter circuit and solve it, which is also the reason why the number of candidate signals cannot be selected in large quantities. It is necessary to reduce the number of candidate signals at the outset.

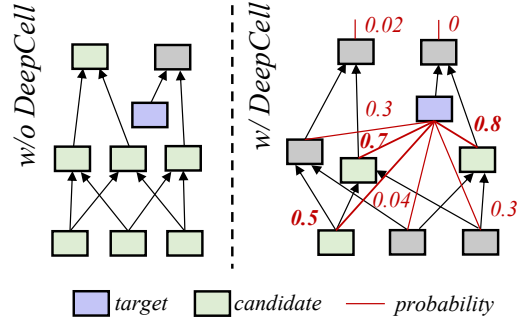


Fig. 4. Select candidate signal with DeepCell

B. Model Finetuning

DeepCell is pretrained to capture the correlation between masked PM netlist and complete AIG. Intuitively, the original circuit that requires patch insertion in ECO task is treated as PM netlist with masking, while the golden circuit provide the complete view. We then finetune DeepCell to effectively learn and represent the relationship between these two circuits.

Therefore, we finetune DeepCell to reduce the space of candidate signals in the ECO process. Specifically, given a PM netlist \mathcal{G}^P , we randomly select a cell p within the netlist and remove its entire driven cone from this node to PI. The removed area, $\mathcal{M}(p)$, is treated as the ground-truth path in ECO. Consequently, the patch-removed netlist is denoted as $\tilde{\mathcal{G}}^P$, while the corresponding AIG netlist for the original PM netlist is denoted as \mathcal{G}^A . Next, we use the PM encoder to encode both patch-removed netlist $\tilde{\mathcal{G}}^P$ and the original netlist \mathcal{G}^P , as denoted in Eq. (13). The AIG encode is employed to encode the AIG netlist \mathcal{G}^A , which serves as the reference ground-truth implementation. The embeddings of the patch-removed netlist are then refined using the AIG embeddings, as described in Eq.(7), to produce the refined embeddings $\tilde{\mathbf{H}}^P$.

$$\begin{aligned}
 \mathbf{H}^A &= \text{DeepGate2}(\mathcal{G}^A) \\
 \mathbf{H}^P &= \text{encoder}(\mathcal{G}^P) \\
 \tilde{\mathbf{H}}^P &= \text{encoder}(\tilde{\mathcal{G}}^P) \\
 \{\mathbf{H}^A, \tilde{\mathbf{H}}^{P'}\} &= \mathcal{T}(\{\mathbf{H}^A, \tilde{\mathbf{H}}^P\})
 \end{aligned} \tag{13}$$

The finetuning tasks are defined as patch reconstruction and driven signal identification. First, in the ideal scenario, the finetuned model should recover the embeddings of the patch with the correct functionality, as informed by the AIG view. We treat the embeddings of the original netlist (prior to patch removal) as the ground truth and define the patch reconstruction loss, $loss_{pr}$ as specified in Eq. (14) (see Fig. 3). We finetune DeepCell using only 8,000 circuits over 10 epochs with loss function $L = loss_{pr} + loss_{drv}$.

$$loss_{pr} = L1Loss(H_i^{P'}, \tilde{H}_i^{P'}), i \in \mathcal{M}(p) \tag{14}$$

Second, in the driven signal identification task, we utilize the refined embeddings to predict whether a given cell is driven by the selected cell p .

$$loss_{drv} = BCELoss(MLP(\{\tilde{H}_i^{P'}, \tilde{H}_p^{P'}\}), 0/1), i \in \mathcal{V}^P \tag{15}$$

TABLE III
PERFORMANCE COMPARISON BETWEEN W/ DEEPCELL AND W/O DEEPCELL ON ICCAD'17 CAD CONTEST BENCHMARKS

Circuit name	PI	PO	Circuit information			<i>w/o DeepCell</i>			<i>w/ DeepCell</i>		
			gate(F)	gate(G)	target	cost	gate	time(s)	cost	gate	time(s)
unit 1	3	2	6	6	1	4	1	0.37	4	1	0.37
unit 2	157	64	1120	1219	1	17	4	0.92	17	4	1.01
unit 3	411	128	2074	1929	1	80	3	0.46	80	3	0.4
unit 4	11	6	75	77	1	32	5	0.49	32	2	0.55
unit 5	450	282	24357	21056	2	47	30	46.3	47	29	15.39
unit 6	99	128	13828	11812	2	-	-	-	-	-	-
unit 7	207	24	2944	1721	1	284	2	8.5	284	2	6.88
unit 8	179	64	2513	3337	1	78	4	4.1	78	3	3.17
unit 9	256	245	5849	4657	4	50	35	1.33	50	26	1.7
unit 10	32	129	1581	1956	2	-	-	-	-	-	-
unit 11	48	50	2057	2160	8	4142	1063	7200	2312	746	6975.3
unit 12	46	27	13804	821	1	104	1	1.02	104	1	0.71
unit 13	25	39	369	426	1	3467	9	1.5	3467	9	1.33
unit 14	17	15	1981	1006	12	95	41	5.43	95	41	6.72
unit 15	198	14	1886	2262	1	191	11	1.93	191	11	0.73
unit 16	417	214	2371	9324	2	278	15	16.58	204	9	14.67
unit 17	136	31	2910	2052	8	434	79	5.04	434	63	6.01
unit 18	245	100	4860	3881	1	18	1	5.14	18	1	2.44
unit 19	99	128	13349	10787	4	-	-	-	-	-	-
unit 20	1874	7105	30876	34002	4	136	6	0.6	120	5	1.12
Geomean						112.36	8.96	3.72	105.83	7.60	3.19
Imp.						1	1	1x	0.06	0.15	0.85x

As shown in Fig. 4, with DeepCell intervention, according to the obtained probability, we remove signals that are almost impossible to drive as targets, so that the number of candidate signals is greatly reduced, so that the situation that needs to be considered in the subsequent steps is controlled in a small range. This operation greatly reduces the running time.

C. Experiment Settings

Our model is equipped into ABC as a plug-in and integrated into the command *'runeco'*, which is an efficient SAT-based solution that won the first place in the 2017 ICCAD contest problem A and added the SAT-based exact pruning method [19]. Usually, the number of signals used in the patches generated by the ECO problem is not so much. In the subsequent experiments, the maximum number of candidate signals we selected is 1000. In [19], the quantified Boolean formula (QBF) method that can be used when the SAT-based feasibility calculation time exceeds the range is introduced. DeepCell, as a generic plug-in, can also be added to these processes if the method code is open source.

D. Main Results

We verify the effectiveness of our model in the 2017 ICCAD contest problem A [21]. These benchmarks are using ISCAS-85/89 [22], ITC-99 [23], IWLS-2005 [24], OpenCore and LGSynth-93 benchmarks and real-world ECO problems from industrial design. As shown in Table III, the sections labeled *'gate(F)'* and *'gate(G)'* correspond to the number of gates in the original circuit and the golden circuit, respectively. The *'w/o DeepCell'* and *'w/ DeepCell'* sections lists the effects of *'runeco'* before and after inserting DeepCell. We limit the maximum running time to two hours. These timeout units are labeled as '-'. It should be denoted that the time reported in the table includes both model inference time and ECO

TABLE IV
PERFORMANCE COMPARISON BETWEEN W/ DEEPCELL AND W/O DEEPCELL ON FIND FEASIBLE ECO SOLUTION

Circuit name	<i>w/o DeepCell</i>			<i>w/ DeepCell</i>		
	cost	support size	time(s)	cost	support size	time(s)
unit 6	-	-	>12600	2500	42	538.06
unit 10	63	16	48.64	63	16	29.2
unit 11	54	3	3977.58	36	2	2379.78
unit 19	-	-	>12600	-	-	>12600

tool runtime. All experiments are performed on a single core of 2.10 GHz Intel(R) Core(TM) i7-14700F CPU with 32GB memory.

From Table III, we can observe that that integrating our DeepCell into the ECO tool achieves significant improvements. Specifically, it reduces the average cost of patches by 6% and the average number of gates by 15%. Additionally, the required runtime decreases by 15%, with no units experiencing increased costs or gate counts. Notably, in the top-performing unit 16, our model achieves a remarkable 27% reduction in cost and a 40% reduction in gate count. These results are attributed to the ability of effectively capturing node relationships, enabling it to calculate the probability of each node for every target in multi-target units.

For small and easy cases (unit 1-4), incorporating DeepCell may slightly increase the runtime due to the high proportion of model inference time. However, as the circuit size increases, the number of potential candidate nodes can be significantly reduced by utilizing the probabilities provided by DeepCell, which in turn accelerates the process. As a result, out of 20 units, the running time increased in 10 instances. The most efficient application (unit 5) achieved a 70% reduction in runtime, while the least efficient case only saw an increase of 0.52 seconds (unit 20).

For four units that encountered timeout and large runtime

(unit 6, 10, 11, 19), we conduct further analysis in Table IV. Data regarding the cost, support size, and runtime for the patches created for the first target of these units are collected. We increase the limit time of this part of the test to three and a half hours. Except for unit 19, the other three units are able to provide a viable solution more quickly, and the quality of these solutions are superior.

VI. CONCLUSION

We introduced DeepCell, a multiview representation learning framework for PM netlists. By integrating a GNN-based PM encoder with a pretrained AIG encoder, and leveraging the novel Mask Circuit Modeling mechanism, DeepCell captures rich and generalizable embeddings of PM netlists. Our experimental results demonstrate the effectiveness of DeepCell in functional ECO, achieving significant reductions in patch generation costs, gate count, and runtime. Future work will explore its adaptability to other critical EDA tasks and extend its scalability to industrial-scale designs.

REFERENCES

- [1] M. Li, S. Khan, Z. Shi, N. Wang, H. Yu, and Q. Xu, "Deepgate: Learning neural representations of logic gates," in *Proceedings of the 59th ACM/IEEE Design Automation Conference*, 2022, pp. 667–672.
- [2] Z. Shi, H. Pan, S. Khan, M. Li, Y. Liu, J. Huang, H.-L. Zhen, M. Yuan, Z. Chu, and Q. Xu, "Deepgate2: Functionality-aware circuit representation learning," in *2023 IEEE/ACM International Conference on Computer Aided Design (ICCAD)*. IEEE, 2023, pp. 1–9.
- [3] Z. Wang, C. Bai, Z. He, G. Zhang, Q. Xu, T.-Y. Ho, B. Yu, and Y. Huang, "Functionality matters in netlist representation learning," in *Proceedings of the 59th ACM/IEEE Design Automation Conference*, 2022, pp. 61–66.
- [4] N. Wu, Y. Li, C. Hao, S. Dai, C. Yu, and Y. Xie, "Gamora: Graph learning based symbolic reasoning for large-scale boolean networks," in *2023 60th ACM/IEEE Design Automation Conference (DAC)*. IEEE, 2023, pp. 1–6.
- [5] C. Deng, Z. Yue, C. Yu, G. Sarar, R. Carey, R. Jain, and Z. Zhang, "Less is more: Hop-wise graph attention for scalable and generalizable learning on circuits," *arXiv preprint arXiv:2403.01317*, 2024.
- [6] J. Devlin, "Bert: Pre-training of deep bidirectional transformers for language understanding," *arXiv preprint arXiv:1810.04805*, 2018.
- [7] S.-L. Huang, W.-H. Lin, P.-K. Huang, and C.-Y. Huang, "Match and replace: A functional eco engine for multierror circuit rectification," *IEEE Transactions on Computer-Aided Design of Integrated Circuits and Systems*, vol. 32, no. 3, pp. 467–478, 2013.
- [8] L. Chen, Y. Chen, Z. Chu, W. Fang, T.-Y. Ho, R. Huang, Y. Huang, S. Khan, M. Li, X. Li *et al.*, "Large circuit models: opportunities and challenges," *Science China Information Sciences*, vol. 67, no. 10, pp. 1–42, 2024.
- [9] Z. Shi, M. Li, S. Khan, L. Wang, N. Wang, Y. Huang, and Q. Xu, "Deeppti: Test point insertion with deep reinforcement learning," in *2022 IEEE International Test Conference (ITC)*. IEEE, 2022, pp. 194–203.
- [10] S. Khan, Z. Shi, M. Li, and Q. Xu, "Deepseq: Deep sequential circuit learning," in *2024 Design, Automation & Test in Europe Conference & Exhibition (DATE)*. IEEE, 2024, pp. 1–2.
- [11] J. Jaeger, "Virtually every asic ends up an fpga," *EE Times*, 2007.
- [12] T. N. Kipf and M. Welling, "Semi-supervised classification with graph convolutional networks," *arXiv preprint arXiv:1609.02907*, 2016.
- [13] P. Veličković, G. Cucurull, A. Casanova, A. Romero, P. Lio, and Y. Bengio, "Graph attention networks," *arXiv preprint arXiv:1710.10903*, 2017.
- [14] F. Brglez, D. Bryan, and K. Kozminski, "Notes on the iscas'89 benchmark circuits," *North-Carolina State University*, 1989.
- [15] S. Davidson, "Characteristics of the itc'99 benchmark circuits," in *ITSW*, 1999.
- [16] L. Amarú, P.-E. Gaillardon, and G. De Micheli, "The eplf combinational benchmark suite," in *IWLS*, no. CONF, 2015.
- [17] T. Edwards, "Introduction to the skywater pdk: The new age of open source silicon," tech. rep, Tech. Rep., 2021.
- [18] J. Liu, J. Zhai, M. Zhao, Z. Lin, B. Yu, and C. Shi, "Polargate: Breaking the functionality representation bottleneck of and-inverter graph neural network," in *2024 IEEE/ACM International Conference on Computer Aided Design (ICCAD)*. IEEE, 2024, pp. 1–9.
- [19] A. Q. Dao, N.-Z. Lee, L.-C. Chen, M. P.-H. Lin, J.-H. R. Jiang, A. Mishchenko, and R. Brayton, "Efficient computation of eco patch functions," in *Proceedings of the 55th Annual Design Automation Conference*, 2018, pp. 1–6.
- [20] B.-H. Wu, C.-J. Yang, C.-Y. Huang, and J.-H. R. Jiang, "A robust functional eco engine by sat proof minimization and interpolation techniques," in *2010 IEEE/ACM International Conference on Computer Aided Design (ICCAD)*. IEEE, 2010, pp. 729–734.
- [21] C. Huang, C. Hsu, and C. Wu, "2017 iccad cad contest problem a: Resource-aware patch generation," in *Proc. ICCAD*, 2017.
- [22] F. Brglez, D. Bryan, and K. Kozminski, "Combinational profiles of sequential benchmark circuits," in *1989 IEEE International Symposium on Circuits and Systems (ISCAS)*. IEEE, 1989, pp. 1929–1934.
- [23] S. Davidson, "Characteristics of the itc'99 benchmark circuits," in *IEEE International Test Synthesis Workshop (ITSW)*, 1999, p. 87.
- [24] C. Albrecht, "Iwls 2005 benchmarks," in *International Workshop for Logic Synthesis (IWLS)*, vol. 9, 2005.